Environmental Pollution 357 (2024) 124413

Contents lists available at ScienceDirect

Environmental Pollution

journal homepage: www.elsevier.com/locate/envpol

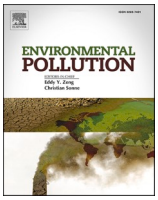

Thallium in Technosols from Allchar (North Macedonia): Isotopic and speciation insights☆

Aleš Vaněk [a,*], Tamara Đorđević [b,c], Martin Mihaljevič [d], Maria Vaňková [d], Karolína Fizková [d], Tereza Zádorová [a], Petra Vokurková [a], Ivana Galušková [a], Vít Penížek [a], Ondřej Drábek [a], Goran Tasev [e], Todor Serafimovski [e], Ivan Boev [e], Blažo Boev [e]

[a] Department of Soil Science and Soil Protection, Faculty of Agrobiology, Food and Natural Resources, Czech University of Life Sciences Prague, Kamýcká 129, 165 00 Praha 6, Czech Republic
[b] 1E057-02 USTEM, Vienna University of Technology, Stadionallee 2, 1020 Vienna, Austria
[c] Department of Mineralogy and Crystallography, University of Vienna, Althanstr. 14, A-1090 Wien, Austria
[d] Institute of Geochemistry, Mineralogy and Mineral Resources, Faculty of Science, Charles University, Albertov 6, 128 00 Praha 2, Czech Republic
[e] Faculty of Natural Sciences, University "Goce Delčev"- Štip, Goce Delčev 89, 2000 Štip, Macedonia

ARTICLE INFO

Keywords:
Soil
Mining
Waste
Isotope
Fractionation
Oxide

ABSTRACT

Allchar (North Macedonia) mining area is known for anomalous background Tl concentrations. In this study, we combine accurate detection of Tl stable isotope ratios with data on mineralogy/speciation and chemical extraction of Tl in Tl-contaminated Technosol profiles. We demonstrate that Tl in the studied soils varies significantly in both concentration (500 mg/kg-18 g/kg) and isotopic composition (−1.6 and +3.2 of ε^{205}Tl, a ~0.5‰ spread), which is due to changes in the phase chemistry and/or mineralogy of Tl. Moreover, the observed $^{205}Tl/^{203}Tl$ ratios do not reflect the extent to which individual soils undergo Tl isotopic fractionation during mineral weathering and soil formation. Clearly, they reflect the initial isotopic signal(s) of the primary ore or ore minerals, and thus, the general history or type of their genesis. As the Tl carriers, various types of Tl–Me-arsenates, mixtures of jarosite and dorallcharite and minor Mn-oxides predominated. We revealed intense adsorption of Tl by the identified Mn-oxides (≤6.7 at.%). It is hypothesized that these phases are of key importance in the fractionation of Tl isotopes, meaning at this type of secondary oxide-soil solution interface. However, model studies involving primary/secondary components (sulfides, sulfates, oxides and arsenates) are required to understand the mechanisms that may lead to post-depositional Tl isotopic redistribution in soils, as well as Tl isotope systematics in mining wastes in general.

1. Introduction

Thallium (Tl) is a highly toxic trace element that can accumulate in different minerals or even form Tl-minerals. Typical primary minerals that can contain up to hundreds of ppm of Tl are mostly sulfides such as sphalerite (ZnS), pyrite (FeS_2), and galena (PbS) (Aguilar-Carrillo et al., 2018; Garrido et al., 2020; Gomez-Gonzalez et al., 2015; Jakubowska et al., 2007; Karbowska et al., 2014; Kersten et al., 2014; Liu et al., 2016, 2019, 2020, 2022; Lukaszewski et al., 2018; Tremel et al., 1997; Vaněk et al., 2016, 2018; Wei et al., 2021; Xiao et al., 2004a,b, 2012 etc.). There are environmental risks arising from the release of Tl during sulfide mining and processing, but also from weathering of various types of Tl-bearing minerals and mining waste. Several individual processes can affect the fate of Tl in the environment, including phase changes, Tl speciation, sorption/coprecipitation reactions etc.

In addition, there are unique ore deposits and mineralizations that are characterized by ore assemblages that are even richer in Tl and where Tl even acts as a mineral-forming element (Lanmuchang and Xiangquan, China; Allchar, North Macedonia; Buus and Lengenbach, Switzerland; Carlin, USA etc.) (Đorđević et al., 2021; Liu et al., 2024; Vaněk et al., 2020; Vejvodová et al., 2022; Voegelin et al., 2015; Xiao et al., 2004a,b, 2012). These areas are probably the most important in terms of studying Tl behavior. Regarding Tl mineralogy, lorándite ($TlAsS_2$), a sulfosalt, is often the major component in these geochemical

☆ This paper has been recommended for acceptance by Dr Hefa Cheng.

* Corresponding author.
E-mail address: vaneka@af.czu.cz (A. Vaněk).

https://doi.org/10.1016/j.envpol.2024.124413
Received 3 April 2024; Received in revised form 29 May 2024; Accepted 19 June 2024
Available online 20 June 2024

anomalies, followed by a number of primary (e.g. fangite, Tl_3AsS_4; raguinite, $TlFeS_2$; picotpaulite, $TlFe_2S_3$; weissbergite, $TlSbS_2$) and secondary minerals (e.g. dorallcharite, $TlFe_3(SO_4)_2(OH)_6$; thallium-pharmacosiderite, $Tl_{2.5}Fe_4[(AsO_4)_3(OH)_4](OH)_{1.5}{\cdot}3H_2O$) (Đorđević et al., 2021; Herrmann et al., 2018; Hettmann et al., 2014; Xiao et al., 2004a,b, 2012).

Only limited information on the systematics of stable Tl isotopes in mining wastes and adjacent soils is available in the literature. Furthermore, there are no studies that would provide both Tl isotopic ($^{205}Tl/^{203}Tl$) and speciation data for these types of anthropogenic samples. A related question is, for example, whether or to what extent mineral weathering and Tl sorption/coprecipitation in the soil may be responsible for changes in Tl isotopic composition. In other words, variations in the $^{205}Tl/^{203}Tl$ ratio can potentially serve as a proxy for understanding these secondary processes, namely Tl accumulation and fixation. Regarding previous studies and related applications of Tl isotopes, these isotopic data have been successfully used for primary source tracing or redox-driven processes in different geosystems such as magmatic and hydrothermal systems, natural sediments/soils, or even specific Tl-bearing phases (e.g., Hettmann et al., 2014; Howarth et al., 2018; Kersten et al., 2014; Liu et al., 2024; Nielsen et al., 2013, 2017; Peacock and Moon, 2012; Phillips et al., 2023; Prytulak et al., 2013, 2017; Rehkämper et al., 2004; Vejvodová et al., 2020 etc.).

Here we present combined results on Tl concentrations, Tl isotopic composition and associated mineralogy obtained in five Technosol profiles developed on Tl-rich wastes from an area of anomalous background Tl content, a mining area in Allchar (North Macedonia). We also attempted to propose the fate/fractionation of Tl isotopes during secondary post-depositional processes where, in addition to the initial Tl isotope signal, phase weathering and/or redox reactions are potentially of key importance.

2. Experimental

2.1. Study area description

The former Sb–As–Tl–Au Allchar deposit is located in the southern part of North Macedonia, on the northwestern edge of the Kozuf Mountains. In terms of its mineralogy, it is one of the most significant ore deposits in the world. It has extremely high Tl grades (500 tonnes) relative to the world's known Tl accumulations. The Allchar deposit was the first Carlin-type gold deposit found in the Balkan Peninsula in the mid-1980s, even containing economically significant concentrations of As and Sb (Percival and Radtke, 1994; Strmić Palinkaš et al., 2018; Volkov et al., 2006). The deposit has been a source of As since the 15th century. Later, with intermittent breaks, it became a source of Sb. In the late 1980s, there was renewed interest in Tl as a potential detector of solar neutrinos, which led to a systematic study of its mineralization in the northern part of this deposit on the Crven Dol ore body (Amthauer et al., 2012; Pavićević et al., 2010). Allchar's mineralization is closely associated with a Pliocene volcanic complex (modified andesite, dacite and latite). The host rocks are mainly Triassic carbonates which are overlain by a Tertiary volcano-sedimentary sequence of tuffs and dolomites. In general, the Allchar mineralization can be divided into the three zones (Janković and Jelenković, 1994): (i) the high-temperature southern zone; (ii) the central zone with Sb and Au dominance, containing As, Tl, minor amounts of Ba, Hg and trace amounts of Pb; and (iii) the northern zone with As–Tl mineralization dominance, containing minor amounts of Sb, Hg and traces of Au. The primary Tl-mineral at Allchar is lorandite ($TlAsS_2$), but ~14 other primary Tl ore minerals have been discovered. With the exception of the Crven Dol locality in the northern part of the deposit (Đorđević et al., 2021), distinctive secondary formations have not yet been fully explored.

2.2. Soil sampling and characterization

Five Technosol profiles developed on mining wastes (gangue; waste rock produced during underground mining) were sampled in this study (in May 2022). The profiles used in this study reflect contrasting geochemical and mineralogical properties. A layer of soil from a depth of 20–30 cm of the naturally developed/uncontaminated profile was used as a reference sample in this study (Fig. S1, Supplementary Material). This uncontaminated/control sample was chosen because of the very low trace element concentrations and a corresponding amount of geogenic Zr, relative to the geochemical situation of Tl in the study area (Vaněk et al., 2016, 2018). Regarding its depth, corresponding to ~B–C horizon, we tried to approximately simulate a moderately weathered soil substrate, i.e., as an analogy to the studied Technosols. The locations of the profiles were chosen so that different mineralogical associations of Tl could potentially be investigated at Allchar (Figs. S1 and S2). In ~0.5 × 1 m wide pits, the soils were sampled in 10-cm depth intervals. In the laboratory, the soil samples were air-dried at room temperature and sieved through a 2-mm stainless steel sieve prior to any further analyses.

Active and exchangeable pH were determined at 1:5 (v/v) ratios of solid sample to H_2O or 1 M KCl solution. Total carbon (TC) and sulfur (TS) concentrations were measured using the catalytic oxidation process (Flash, 2000 Series CNS analyzer, Thermo Scientific, Germany). The cation exchange capacity (CEC) was determined on the basis of Ba^{2+} soil exchange site saturation (0.1 and 0.01 M $BaCl_2$) followed by Ba^{2+} exchange with Mg^{2+} (0.02 M $MgSO_4$) (ISO 11260:2018). Oxalate-extractable Fe, Mn, Al and Tl contents, simulating oxide-associated soil fraction(s), were determined using an acid oxalate extract (0.2 M ammonium oxalate/oxalic acid; pH 3.0) (Pansu and Gautheyrou, 2006). The clay content was determined using the sedimentation method performed on mixed profile samples.

In order to characterize soil mineralogy, selected samples with high Tl/trace element concentrations were analyzed by powder X-ray diffraction (PXRD). Analysis was carried out using Bruker D8 Advance diffractometer (Cu-*K*α radiation, Lynxeye detector, 40 kV, 25 mA, step scanning from 5° to 85° 2θ, room temperature, step size 0.01° 2θ, dwell time of 1 s per step). DIFFRAC.EVA software, version 4.2, and the ICDD powder diffraction file PDF-2 were used for phase identification. As for the Tl speciation in the solid phase, the same group of samples (as for PXRD) was subjected to a combination of scanning electron microscopy with energy dispersive X-ray spectroscopy (SEM-EDX) and micro-Raman spectroscopy. Both SEM-EDX and Raman investigations were performed on the polished sections. Chemical composition and micromorphology of mineral phases were studied using a JEOL JSM-6610 LV scanning electron microscope (SEM) with tungsten filament (15 kV), equipped with an energy-dispersive X-ray (EDX) detector (Bruker e-FlashHR+, resolution 127 eV) and Bruker Esprit 2.0 software. Spectra were recorded for 60 s and with <5% dead times. Raman spectra were measured with a Horiba LabRam-HR system equipped with an Olympus BX41 optical microscope in the spectral range between 100 and 4000 cm^{-1} (632.8 nm He–Ne laser; 50 × or 100 × objective; N.A. = 0.90; exposure time between 10 and 60 s).

Prior to determining Tl/element concentrations and Tl isotopic ratios, soil samples were pulverized in an agate mill (Pulverisette 0, Fritsch, Germany). A mass of 0.2 g of each material was decomposed using an acid mixture in a microwave unit (Multiwave 5000, Anton Paar, Austria). Concentrated HNO_3 and HF mixed in the ratio of 2:1 (Merck Ultrapure, Germany) was used in a total volume of ≤20 mL, the dissolved sample was subsequently transferred into PTFE beakers (Savillex, USA) and evaporated on a hot plate. The remaining solutions were then dissolved in 2% HNO_3 and stored. Selected samples were extracted with 1 M NH_4NO_3 (S/L ratio, 1/10, 2 h) to determine the exchangeable and/or readily mobilizable Tl fractions, simulating a labile Tl pool in soil. This type of extraction is based on a modified method used elsewhere (Vaněk et al., 2020; Vejvodová et al., 2020).

Thallium, Pb, As, Sb, Fe, Mn, Al, Zr and Ca concentrations in the total

soil digests and/or soil extracts were determined using either a quadrupole-based inductively coupled plasma mass spectrometer (Q-ICP-MS, iCAP RQ, Thermo Scientific, Germany) or an inductively coupled plasma optical emission spectrometer (ICP-OES, iCAP 6500, Thermo Scientific, UK) under standard analytical conditions. The standard reference material (SRM) NIST 2711 (Montana Soil) was used for QC of the quantitative analysis. The Tl, As and Pb recovery rates achieved >95% of the certified element concentrations (Table S1).

In order to quantify the overall addition of Tl in the individual soil samples, relative to the reference (uncontaminated) soil in the study area, we used the τ-parameter. This approach enables the identification of the proportion of Tl gained or eventually lost at a specific soil layer, relative to an immobile (conservative) Zr (Eq. (1)); where C is the concentration of Tl and Zr in a given soil layer or a reference sample.

$$\tau_{Tl/Zr} = \frac{(C_{Tl}/C_{Zr})_{sample}}{(C_{Tl}/C_{Zr})_{ref.\ soil}} - 1 \quad (1)$$

2.3. Thallium separation and isotopic measurement

The measurement of Tl isotopic ratios preceded Tl isolation from dissolved sample matrices. For this purpose, a two-stage chromatographic separation using the Bio-Rad AG1-X8 anion exchange resin (200–400 mesh, Cl^- cycle) was conducted. Detailed information about the separation process is available in Grösslová et al. (2018), Vaněk et al. (2016, 2018, 2020) or Vejvodová et al. (2020). The determination of $^{205}Tl/^{203}Tl$ ratios was made using MC-ICP-MS Neptune Plus (Thermo Scientific, Germany) and the analytical conditions similar to those described in e.g. Prytulak et al. (2013, 2017) (see Supplementary Material for details). The Tl isotopic composition was calculated using the following equation with ε notation relative to NIST SRM 997 (Eq. (2)). The presented $\varepsilon^{205}Tl$ values for the studied sample set are assigned the estimated error of ±0.7 (2σ), based on the reproducibility of complete multiple analyses of SRM AGV-2 (Andesite, USGS, USA) (Table S2) within our lab – Isotope Research Center of the Faculty of Science (Charles University, Prague). Therefore, this type of uncertainty accounts for all possible sources of error – sample dissolution, Tl ion

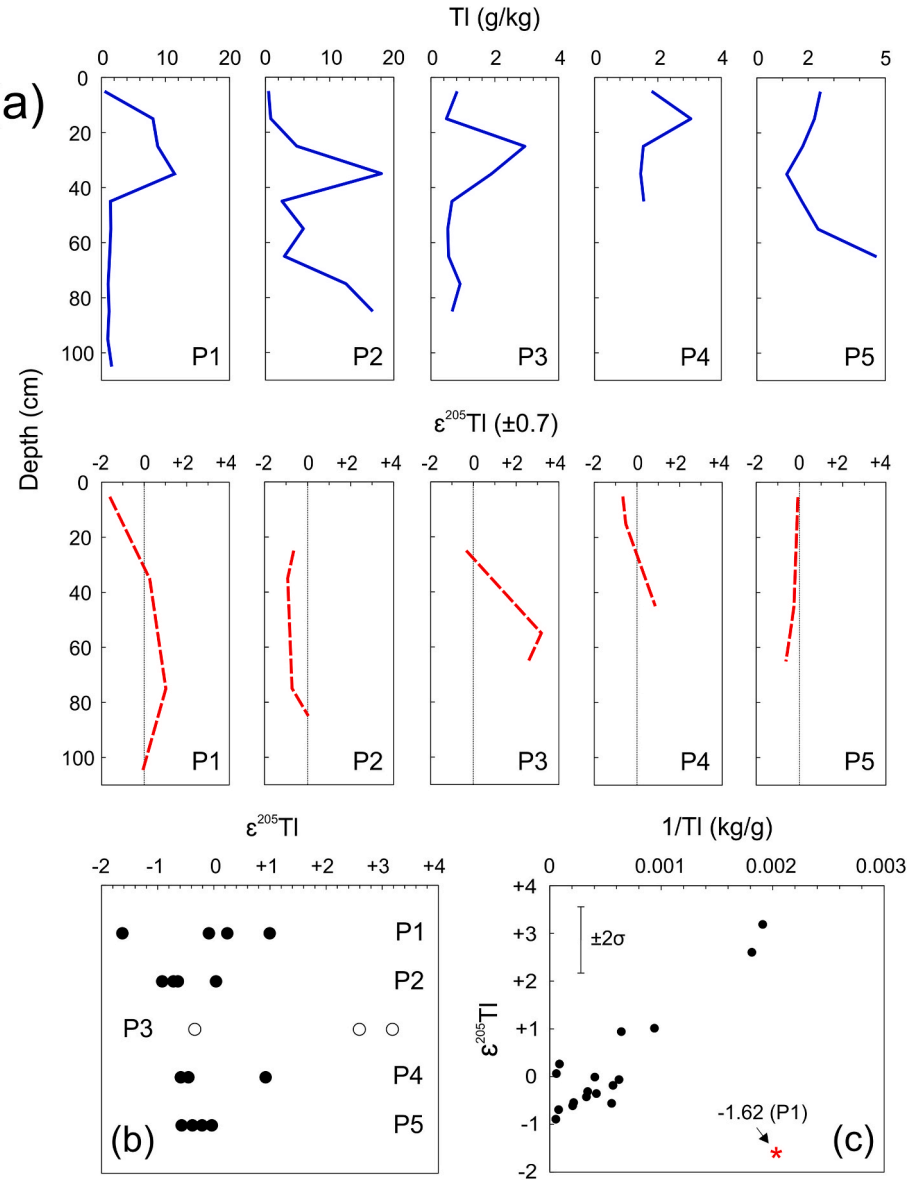

Fig. 1. Depth-dependent evolution of Tl concentration and Tl isotopic signature in the studied Technosol profiles (P1–P5) (a); summary of Tl isotopic data (b); Tl isotopic composition versus inverse Tl concentration (1/Tl) (c). The $\varepsilon^{205}Tl$ data are assigned an error of ±0.7 (2σ), based on our long-term external reproducibility for the SRM AGV-2 (Andesite, USGS, USA); see Supplementary Material for details.

exchange chemistry and mass spectrometry. The QC data obtained for AGV-2 are shown in Table S2.

$$\varepsilon^{205}Tl = \frac{^{205}Tl/^{203}Tl_{sample} - ^{205}Tl/^{203}Tl}{^{205}Tl/^{203}Tl} \times 10^4 \quad (2)$$

3. Results and discussion

3.1. Soil properties and thallium concentrations

To comment briefly on the physicochemical properties of the studied Technosol profiles, all soil samples had low clay content (≤7 wt%) and the majority had neutral to slightly alkaline pH and moderate CEC values (~10–30 cmol/kg) (Table S3). The combination of TC, TS and Ca concentrations clearly indicates both the high content of inorganic C associated with carbonates and the sulfidic and/or sulfate nature of S (Tables 1 and S3).

The total Tl concentrations in Technosol samples were highly variable and ranged from ~500 mg/kg to 18 g/kg, as shown in Fig. 1a and Table 1. This was further reflected by changes in vertical Tl distribution within each soil profile. The combination of the overall patterns of Tl, Fe, As and Sb concentrations and the lack of correlation between them (Tables 1 and S4) confirms the variations of Tl-containing minerals as well as their chemical variability, meaning that they substantially differ in both nature and Tl and trace/major element enrichments. The only exception is an apparent (positive) correlation between As and S, and Tl to some degree, reflecting the sulfidic/sulfate nature of Tl. Since the calculated τ values have a wide range and are mostly very high (15–6000) (Table 1), it is easy to infer to what extent Tl is enriched in the studied Technosols.

With the exception of Profile 5 (P5), we identified large concentration peaks of Tl in subsurface layers of all profiles (P1–P4) (Fig. 1a). This spatial variation indicates downward Tl migration, in the form of particulates, due to soil physical processes. Moreover, it is reasonable to expect movement of dissolved forms of Tl. This is evidenced by the large proportion of the labile/exchangeable Tl fraction (extracted by NH_4NO_3) in selected samples (profiles P1 and P2), corresponding to

Table 1
Total Tl, Zr, Pb, As, Sb, Fe, Ca, C and S concentrations, exchangeable/labile (NH_4NO_3-extractable) Tl concentrations, Tl enrichments and Tl isotopic compositions (in ε^{205}Tl) in the studied Technosol profiles and the reference soil.

Soil profile	Layer (depth, cm)	Tl (mg/kg)	Tl_{NH4NO3} (mg/kg)	ε^{205}Tl (±0.7)	Zr (mg/kg)	Tl/Zr	τ-value	Pb (mg/kg)	As (mg/kg)	Sb (mg/kg)	Fe (mg/kg)	Ca (mg/kg)	C (wt. %)	S (wt. %)
P1	0–10	492	51	−1.628	140	4	15	121	3690	12	29600	32400	1.61	0.35
	10–20	8050	–	–	21.1	381	1726	31	38600	127	39400	167000	8.17	1.72
	20–30	8780	–	–	10.6	832	3770	25	44100	152	35800	171000	8.53	1.60
	30–40	11400	200	+0.241	13.6	841	3813	20	41800	100	52000	173000	8.47	0.19
	40–50	1420	–	–	2.60	543	2459	4	18100	122	7950	272000	10.9	0.13
	50–60	1480	–	–	<DL	–	–	3	18300	129	7100	265000	10.5	0.26
	60–70	1290	–	–	2.66	485	2200	8	11300	130	6350	270000	10.7	0.11
	70–80	1060	117	+0.995	4.12	258	1171	3	10200	125	5450	292000	10.9	0.04
	80–90	1200	–	–	76.0	16	70	3	11900	154	6300	282000	10.7	0.90
	90–100	988	–	–	5.01	197	892	4	12900	173	6950	280000	10.6	0.81
	100–110	1610	126	−0.088	13.2	122	554	4	16000	219	7550	265000	10.9	0.49
P2	0–10	459	–	–	24.5	19	84	31	4330	31	8750	172000	11.8	0.01
	10–20	807	–	–	35.3	23	103	29	10400	115	14100	161000	10.0	0.24
	20–30	4860	124	−0.639	63.2	77	348	68	41700	355	31700	123000	7.07	0.90
	30–40	18100	859	−0.919	75.6	239	1083	82	254000	2570	42100	7700	0.48	6.10
	40–50	2570	–	–	79.5	32	146	72	336000	1960	32100	2600	0.28	9.71
	50–60	5900	–	–	112	53	238	108	439000	3200	42000	9570	0.25	9.30
	60–70	2940	–	–	291	10	45	53	296000	1580	36400	17800	0.26	9.33
	70–80	12500	1071	−0.720	37.2	337	1528	62	256000	1270	44900	38800	0.36	9.14
	80–90	16700	2239	+0.039	30.8	543	2460	49	133000	1190	35100	41300	0.25	7.25
P3	0–10	820	–	–	11.9	69	312	75	13000	2260	29400	98500	6.98	0.68
	10–20	482	–	–	2.42	199	901	15	7880	1800	16200	131000	8.19	0.03
	20–30	2940	11	−0.339	18.0	163	739	44	35000	5240	49700	33200	1.86	0.80
	30–40	1890	–	–	6.77	279	1266	35	35900	5750	51000	69100	3.73	1.94
	40–50	653	–	–	16.3	40	181	17	14700	22700	46900	133000	7.04	2.27
	50–60	523	39	+3.181	0.39	1335	6052	8	8770	13800	46600	169000	9.10	1.39
	60–70	551	56	+2.593	<DL	–	–	10	10300	6060	37700	165000	9.52	0.75
	70–80	912	–	–	13.8	66	298	28	33000	3800	54500	120000	6.47	1.82
	80–90	660	–	–	38.9	17	76	44	15000	6110	44400	90100	4.76	1.61
P4	0–10	1800	12	−0.589	41.3	44	197	52	43700	4560	54500	16200	1.08	0.54
	10–20	3040	8	−0.452	51.9	59	265	94	41900	4390	36500	10800	0.44	1.05
	20–30	1540	–	–	30.6	50	227	53	37700	13100	70500	30100	0.63	2.53
	30–40	1460	–	–	29.9	49	220	49	33300	18300	75500	38300	0.71	3.05
	40–50	1560	25	+0.924	27.5	56	255	46	44700	7990	73000	58800	1.49	3.89
P5	0–10	2470	29	−0.036	19.8	125	564	54	31500	23600	74500	32000	2.20	0.94
	10–20	2240	–	–	22.3	101	455	58	29800	20800	72500	22900	1.64	0.86
	20–30	1780	–	–	22.8	78	354	67	22700	14400	52500	18900	0.38	2.00
	30–40	1160	–	–	7.52	155	700	30	17500	8780	67500	89300	3.31	4.48
	40–50	1760	33	−0.210	14.1	125	566	23	12400	47200	29300	31300	0.36	3.03
	50–60	2390	65	−0.381	16.6	144	652	29	8530	50600	23100	28000	0.15	3.05
	60–70	4660	62	−0.572	12.9	363	1644	39	24500	38600	78500	48500	0.34	4.67
Ref. soil	20–30	17.0	–	+0.505	76.7	0.2	–	130	408	3	24400	14500	0.65	0.17

Average concentrations (n = 2); RSD <10% (1σ). –: not determined. <DL: below detection limit.
The ε^{205}Tl data are assigned an error of ±0.7 (2σ); see Sections 2.3 and III (Supplementary Material) for details.
The τ parameter was calculated as follows: (Tl/Zr)soil/(Tl/Zr)ref. soil – 1; τ > 0 indicates Tl enrichment.
Ref. soil: reference soil represents an uncontaminated sample from a depth of 20–30 cm in a naturally developed soil profile (Fig. S1, Supplementary Material).

≤13% of the total Tl content (Table 1). On the other hand, this process cannot be as significant considering our clay-depleted sandy soils (Table S3), which facilitates the vertical migration of Tl-rich (micro) particles. Similarly, the depositional history and/or characteristic soil mixing in most profiles cannot explain comparable vertical trends in Tl. It is important to note that NH_4NO_3-extractable Tl concentrations ranged widely (8–2200 mg/kg) (Table 1), but it was difficult to unambiguously link this fraction to a single soil factor. However, it seems that NH_4NO_3-extractable Tl and low pH are factors that accompany high concentrations of total Tl in the studied soils (Tables 1 and S3). Regarding the oxalate-extractable Mn and Tl concentrations, representing soil fraction(s) bound to oxides, there is evidence of their correlation in Profile 1 ($R^2 > 0.9$; n = 4) (Table S3). At this point, it should be noted that the role of Mn-oxides in Tl uptake, via simple (non-specific) sorption, Tl(I)–K(I) ion exchange or oxidative Tl sorption onto these phases, is well established and has been reported as a key control in the sequestration of mobile/mobilized Tl in all mining waste, soil and sedimentary systems (Aguilar-Carrillo et al., 2018; Howarth et al., 2018; Nielsen et al., 2013, 2017; Peacock and Moon, 2012; Rehkämper et al., 2004; Vaněk et al., 2020; Vejvodová et al., 2020; Voegelin et al., 2015; Wick et al., 2019, 2020). Additional evidence for the proposed association of Tl and Mn-oxides in respective soil samples is provided by Tl speciation data (see Section 3.3).

3.2. Sample mineralogy

Regarding bulk soil mineralogy, the samples mostly consist of dolomite ($CaMg(CO_3)_2$), calcite ($CaCO_3$), quartz (SiO_2), K-feldspar ($KAlSi_3O_8$), muscovite ($KAl_2(AlSi_3O_{10})$ $(F,OH)_2$), gypsum ($CaSO_4{\cdot}2H_2O$), kaolinite ($Al_2Si_2O_5(OH)_4$) and illite ($(K,H_3O)Al_2(Si,Al)_4O_{10}(OH)_2$). Additionally, orpiment (As_2S_3), realgar (As_4S_4), jarosite ($KFe^{3+}_3(SO_4)_2(OH)_6$), scorodite ($FeAsO_4{\cdot}2H_2O$), dorallcharite ($TlFe^{3+}_3(SO_4)_2(OH)_6$) with traces of pharmacosiderite ($KFe^{3+}_4(AsO_4)_3(OH)_4{\cdot}6–7H_2O$) and arseniosiderite ($Ca_2Fe^{3+}_3(AsO_4)_3O_3{\cdot}3H_2O$) represented major As/Fe/(Tl)-phases containing Tl, as detected by PXRD (Figs. S3–S7).

3.3. Thallium speciation

The combination of SEM-EDX and Raman spectroscopic data shows generally consistent results with those obtained by PXRD. The most important findings on Tl speciation are shown in Fig. 2. Some concentration data and details on Tl/metal speciation from individual soil profiles are given in Supplementary Material (Figs. S8–S15 and Tables S5–S8).

As for Profile 1, the primary source of Tl is lorándite ($TlAsS_2$), which is frequently found inter-grown with realgar (Fig. S8a). Thallium dissolved during weathering is reprecipitated as dorallcharite (Fig. S9a), which crystallizes as small spherulitic aggregates embedded in hydrous ferric oxides (HFO). Thallium even accumulates in Mn-oxides that contain Tl, Ca, and As (1.9–6.7 at.% Tl; 0.4–6.9 at.% Ca; 0.1–4.4 at.% As) (Fig. 2d–S9b,f and Table S5) and thalliumpharmacosiderite ($TlFe_4(AsO_4)_3(OH)_4{\cdot}4H_2O$) (Figs. S9c and d). However, the most common Tl-bearing precipitates in this profile are Tl–Me^{2+}-arsenates (Me^{2+} = Ca, Mn, Mg, Fe) with varying Tl:Me:As ratios (Figs. S9e and f and Table S5). Raman spectroscopy was used to further investigate thallium metal arsenates. This resulted in quite broad Raman shifts in two major spectral ranges, 350–600 and 700-900 cm^{-1} (Fig. S10). Similarly to Tl-arsenates described by Đorđević et al. (2021), both spectral ranges are attributed to arsenate tetrahedra showing As–O symmetric bending and stretching modes for the two regions, respectively.

As for Profile 2, it was revealed that the main primary sources of Tl are lorándite, which appears as strongly weathered aggregates, rebulite ($Tl_5Sb_5As_8S_{22}$) and raguinite ($TlFeS_2$) (Fig. S11), both embedded in orpiment crystals. The dissolved Tl has been precipitated in the form of jarosite-group minerals that form solid solution between pure jarosite and Tl-bearing jarosite to pure dorallcharite, which is the primary Tl-precipitate in the P2-samples. Tl-bearing jarosites were accompanied by Al-bearing scorodite (3.1 at.% of Al) and pure mansfeldite ($AlAsO_4{\cdot}H_2O$) (Fig. S12 and Table S6).

For the remaining profiles (P3–P5), Sb type of associated mineralization prevails, along with As and Tl. We were unable to detect any primary Tl-minerals in the respective soil samples under investigation. Only the remains of highly weathered Tl- and Hg-bearing sulfosalts embedded in realgar could be observed. Other primary phases, including pyrite/marcasite, arsenopyrite, realgar, and stibnite, are all heavily weathered. Thallium dissolved during weathering is reprecipitated as Tl-bearing jarosite or K-bearing dorallcharite, with Tl concentrations as high as 2.8 at.% (Figs. S13–15 and Tables S7 and S8).

3.4. Thallium isotopic composition

The Tl isotopic ratios (in $\varepsilon^{205}Tl$) determined in the studied profiles are listed in Table 1 and shown in Fig. 1a and b. As a sample set, they were variable, with $\varepsilon^{205}Tl$ ranging between −1.6 and + 3.2, a ~0.5‰ spread. For comparison, the $\varepsilon^{205}Tl$ value found for the reference soil sample accounted ~+0.5 (Table 1). In addition, each profile showed a specific isotopic pattern in the soil layers which was not uniform. On the other hand, the variations in the Tl isotopic signature were relatively low for Profile 2, corresponding to ~1 $\varepsilon^{205}Tl$ unit, and only minimal for Profile 5 (~0.5 $\varepsilon^{205}Tl$ unit) (Fig. 1a and b). Therefore, the isotopic variability of the latter profile was lower than the estimated procedural error (2σ) for our dataset. The largest depth-dependent changes in $\varepsilon^{205}Tl$, from −0.3 to +3.2, a 0.35‰ spread, were observed in Profile 3 (Fig. 1a and b). It is clear that the determined $^{205}Tl/^{203}Tl$ ratios reflect isotopic variations in primary Tl-containing minerals with varying Tl/element chemistry, thus generally the history or type of their hydrothermal genesis. The formation of Tl-rich weathering products (precipitates) may have led in part to secondary fractionation of Tl isotopes. However, their role cannot be as significant since they cannot lead to detectable $\varepsilon^{205}Tl$ shifts in soil layers that are simultaneously highly variable in both element and phase compositions (see last two paragraphs).

In general, the $^{205}Tl/^{203}Tl$ ratio can vary over several generations of local ore minerals following the fact that the isotopic signal of available Tl in hydrothermal solutions can also readily change (Hettmann et al., 2014; Prytulak et al., 2013, 2017). Leaving aside Tl, these types of systematics have recently been observed in other isotope systems, namely Ag and Cu (Kříbek et al., 2018; Mathur et al., 2009, 2018; Wang et al., 2022). Such a phenomenon can be attributed not only to different metal binding or phase chemistry and associated isotopic fractionation, but mainly to the role of the initial metal sources (melt or hydrothermal solution) and their $^{205}Tl/^{203}Tl$ signals. Regarding Ag, for example, Milot et al. (2022) or Wang et al. (2022) report identical large isotopic variability of Ag in PbS (≤6‰) within a single polymetallic system, suggesting a sequence of its formation with significantly different isotopic compositions.

Looking at the plot of 1/Tl versus $\varepsilon^{205}Tl$ (Fig. 1c), a linearity between these two parameters is apparent (except for one P1 sample), indicating a tendency for samples with increasing Tl concentration to be isotopically lighter and vice versa. Consistent with the overall isotopic pattern, a ternary mixing involving one major geogenic Tl pool and two minor Tl pools can potentially be inferred (Fig. 1c). In terms of Tl sources, the $\varepsilon^{205}Tl$ range of −1 and 0 represent the leading isotopic signal in our soils that, in parallel, is clearly prevalent in samples with higher Tl concentrations of ~≥1500 mg/kg (Fig. 1c and Table 1). This also means that the post-depositional isotopic redistribution (fractionation) of Tl caused by weathering of primary minerals and associated sorption/precipitation Tl reactions could not markedly affect the inherited Tl isotopic soil signature(s). Furthermore, the observed $\varepsilon^{205}Tl$ data combined with Tl enrichment (τ factor) (Table 1) provide additional evidence that secondary soil processes alone were not sufficient to induce detectable

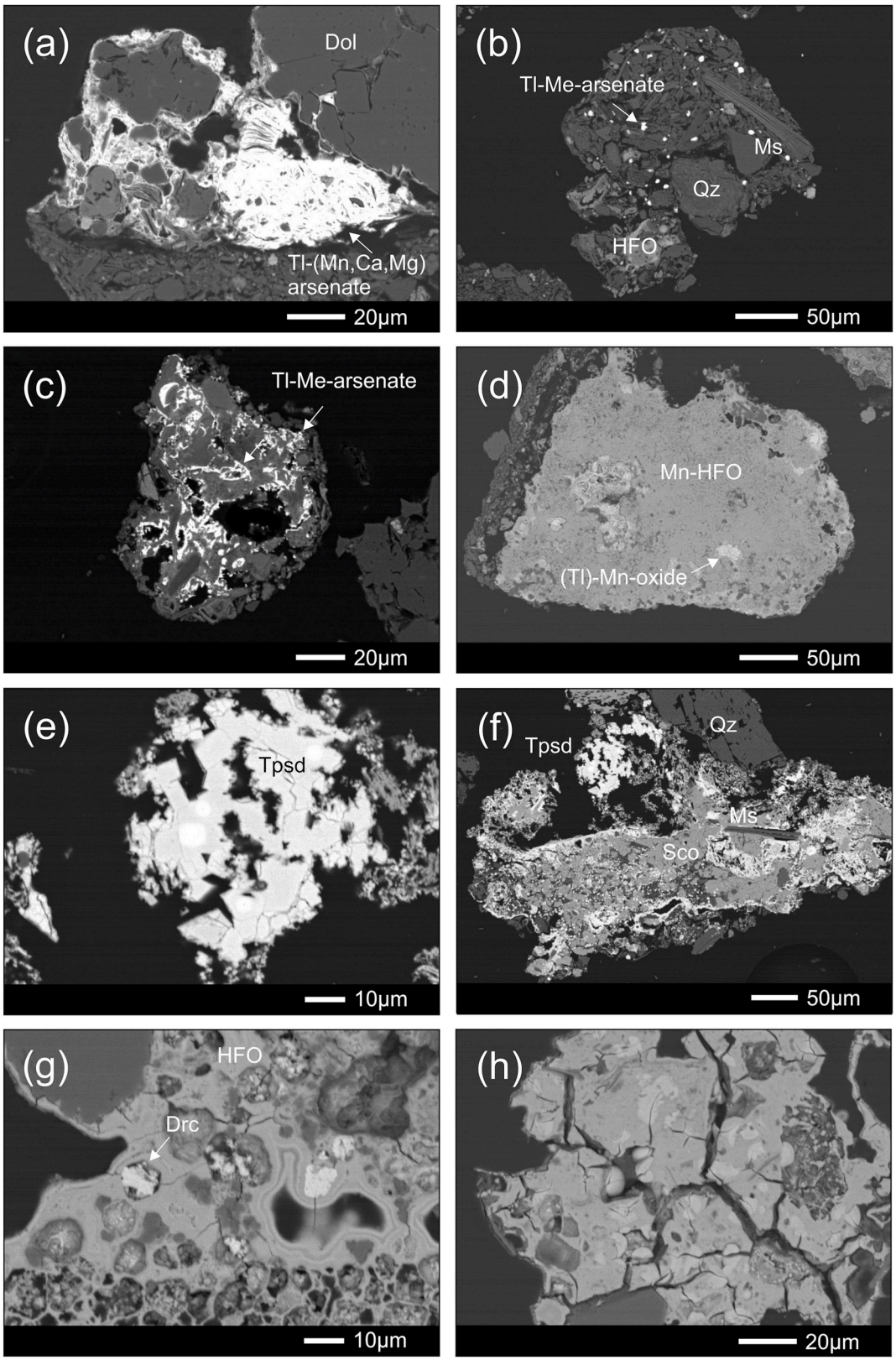

Fig. 2. Scanning electron micrographs (SEM) in back-scattered electrons of selected heavy microparticles (primary + secondary minerals) observed in the studied Technosols. Foliated Tl–Me-arsenate inter-grown with dolomite (a); aggregates of Tl–Me-arsenate and hydrous ferric oxides + quartz and muscovite (b); aggregates of Tl–Me-arsenate mostly in impure Mn-oxide (c); Tl-bearing Mn-oxide (Tl ≤ 6.7 at.%) in Mn-rich hydrous ferric oxides (d); Tl-pharmacosiderite (e); Tl-pharmacosiderite with scorodite + muscovite and quartz (f); dorallcharite occluded in hydrous ferric oxides (g); dorallcharite (bright) in Ca–Fe-arsenate (h). Abbreviations: Dol (dolomite); Qz (quartz); HFO (hydrous ferric oxides); Tpsd (Tl-pharmacosiderite); Drc (dorallcharite); Sco (scorodite); Ms (muscovite). See Supplementary Material for details.

isotopic changes, i.e., in bulk soil samples.

If we consider the sub-processes of Tl at the solid phase-soil solution interface, they are likely to be associated with isotopic fractionation. Acid Tl(I) leaching from primary ore minerals followed by oxidative Tl adsorption seem to represent the key process toward the positive ε^{205}Tl values. Sequestration of Tl by secondary Mn(III,IV)-oxides (hexagonal birnessite and δ-MnO_2), including the precipitation of Tl_2O_3 (avicenite) (Bidoglio et al., 1993; Peacock and Moon, 2012) or even by specific Fe (III)-oxides, are systematically considered to be the primary cause of moderate/high positive ε^{205}Tl anomalies (~≤+10 ε^{205}Tl) in soil/sedimentary systems (Howarth et al., 2018; Liu et al., 2022, 2024; Nielsen et al., 2013, 2017; Rehkämper et al., 2004; Vaněk et al., 2016, 2018; 2020; Vejvodová et al., 2020). Although Tl can also be captured by Mn-oxides in a simpler manner (Voegelin et al., 2015; Wick et al., 2019), i.e., without redox changes, non-oxidative uptake of Tl is not expected to cause significant isotopic effects (Nielsen et al., 2013; Peacock and Moon, 2012). Similarly, a recent laboratory seawater study by Phillips et al. (2023) showed only a small positive variation in ε^{205}Tl upon Tl fixation by triclinic birnessite and todorokite ($\alpha_{adsorbed\text{-}dissolved}$ ≤0.0001), which was not accompanied by any Tl(I) and Mn oxidation shifts, as revealed by X-ray absorption near edge structure spectroscopy (XANES) and PXRD. Although no solid form containing Tl(III) was detected in our samples, the identified Mn-oxide(s) exhibit extreme Tl saturation (≤6.7 at.%), as determined by EDX (Fig. 2 and Table S5). Combining all of the available findings, one can readily deduce the fractionation of Tl isotopes during the Tl–Mn-oxide interactions in Profile 1. However, this assumption remains unproven since we studied the ^{205}Tl/^{203}Tl systematics in the soil layers (bulk samples), not in the reactive microzones.

4. Conclusions

This work combines accurate detection of Tl isotopic ratios with data on Tl concentration, mineralogy, speciation and chemical extractions in Tl-contaminated Technosol profiles (Allchar, North Macedonia). Here we show that Tl in the studied soils varies significantly in both concentration (500 mg/kg-18 g/kg) and isotopic composition (−1.6 and +3.2 of ε^{205}Tl, a ~0.5‰ spread), resulting from changes in phase chemistry and/or mineralogy of Tl. Furthermore, the observed ^{205}Tl/^{203}Tl ratios do not reflect the extent to which individual soil layers (soil profiles) undergo Tl isotopic fractionation during mineral weathering and soil formation. Clearly, they are largely inherited, i.e., they reflect the initial isotopic composition in the primary ores or ore minerals. On the other hand, inverse 1/Tl concentrations versus Tl isotopic data show that in most soil samples the leading signal falls in the ε^{205}Tl range between −1 and 0. As the Tl carriers, various types of Tl–Me-arsenates, mixtures of jarosite and dorallcharite and minor Mn-oxides predominated. Using chemical and mineralogical methods, we even revealed intense adsorption of Tl by the identified Mn-oxides. We hypothesize that these phases are of key importance in the fractionation of Tl isotopes, at this type of oxide-soil solution interface. However, model studies involving primary/secondary components (sulfides, sulfates, oxides and arsenates) are required to better understand mechanisms that may influence post-depositional Tl isotopic patterns in soils and mining wastes in general.

CRediT authorship contribution statement

Aleš Vaněk: Writing – original draft, Methodology, Investigation, Conceptualization. **Tamara Đorđević:** Writing – original draft, Methodology, Investigation, Conceptualization. **Martin Mihaljevič:** Writing – review & editing, Investigation. **Maria Vaňková:** Writing – review & editing, Methodology, Investigation. **Karolína Fizková:** Investigation. **Tereza Zádorová:** Methodology, Investigation. **Petra Vokurková:** Investigation. **Ivana Galušková:** Investigation. **Vít Penížek:** Methodology, Investigation. **Ondřej Drábek:** Investigation. **Goran Tasev:** Resources, Conceptualization. **Todor Serafimovski:** Conceptualization. **Ivan Boev:** Resources. **Blažo Boev:** Resources, Conceptualization.

Declaration of competing interest

The authors declare that they have no known competing financial interests or personal relationships that could have appeared to influence the work reported in this paper.

Data availability

Data will be made available on request.

Acknowledgements

This research was funded by the grant of the Czech Science Foundation (23-04891 S) and supported by the Johannes Amos Comenius Programme (P JAC), project No. CZ.02.01.01/00/22_008/0004605, Natural and anthropogenic georisks. T. Đorđević and A. Vaněk also acknowledge the supports of the Austrian Science Fund (FWF) [P 36828-N] and the Ministry of Education, Youth and Sports (MŠMT) [P 8J20AT009]. Marie Fayadová is gratefully thanked for her laboratory assistance. Dr. Christopher Ash (UK) is thanked for English editing. Furthermore, the help of anonymous four reviewers significantly improved the quality of the original manuscript version.

Appendix A. Supplementary data

Supplementary data to this article can be found online at https://doi.org/10.1016/j.envpol.2024.124413.

References

Aguilar-Carrillo, J., Herrera, L., Gutiérrez, E.J., Reyes-Domínguez, I.A., 2018. Solid-phase distribution and mobility of thallium in mining-metallurgical residues: environmental hazard implications. Environ. Pollut. 243, 1833–1845. https://doi.org/10.1016/j.envpol.2018.10.014.

Amthauer, G., Pavićević, M.K., Jelenković, R., Goresy, A., Boev, B., Lazić, P., 2012. State of geoscientific research within the lorándite experiment (LOREX). Mineral. Petrol. 105, 157–169. https://doi.org/10.1007/s00710-012-0209-7.

Bidoglio, G., Gibson, P.N., O'Gorman, M., Roberts, K.J., 1993. X-ray absorption spectroscopy investigation of surface redox transformations of thallium and chromium on colloidal mineral oxides. Geochem. Cosmochim. Acta 57, 2389–2394. https://doi.org/10.1016/0016-7037(93)90576-I.

Đorđević, T., Drahota, P., Kolitsch, U., Majzlan, J., Peřestá, M., Kiefer, S., Stoger-Pollach, M., Tepe, N., Hofmann, T., Mikuš, T., Tasev, G., Serafimovski, T., Boev, I., Boev, B., 2021. Synergetic Tl and as retention in secondary minerals: an example of extreme arsenic and thallium pollution. Appl. Geochem. 135, 105114 https://doi.org/10.1016/j.apgeochem.2021.105114.

Garrido, F., Garcia-Guinea, J., Lopez-Arce, P., Voegelin, A., Göttlicher, J., Mangold, S., Almendros, G., 2020. Thallium and co-genetic trace elements in hydrothermal Fe-Mn deposits of Central Spain. Sci. Total Environ. 717, 137162 https://doi.org/10.1016/j.scitotenv.2020.137162.

Gomez-Gonzalez, M.A., Garcia-Guinea, J., Laborda, F., Garrido, F., 2015. Thallium occurrence and partitioning in soils and sediments affected by mining activities in Madrid province (Spain). Sci. Total Environ. 536, 268–278. https://doi.org/10.1016/j.scitotenv.2015.07.033.

Grösslová, Z., Vaněk, A., Oborná, V., Mihaljevič, M., Ettler, V., Trubač, J., Drahota, P., Penížek, V., Pavlů, L., Sracek, O., Kříbek, B., Voegelin, A., Göttlicher, J., Ondřej, D., Tejnecký, V., Houška, J., Mapani, B., Zádorová, T., 2018. Thallium contamination of desert soil in Namibia: chemical, mineralogical and isotopic insights. Environ. Pollut. 239, 272–280. https://doi.org/10.1016/j.envpol.2018.04.006.

Herrmann, J., Voegelin, A., Palatinus, L., Mangold, S., Majzlan, J., 2018. Secondary Fe-as-Tl mineralization in soils near Buus in the Swiss Jura Mountains. Eur. J. Mineral 30, 887–898. https://doi.org/10.1127/ejm/2018/0030-2766.

Hettmann, K., Kreissig, K., Rehkämper, M., Wenzel, T., Mertz-Kraus, R., Markl, G., 2014. Thallium geochemistry in the metamorphic Lengenbach sulfide deposit, Switzerland: thallium-isotope fractionation in a sulfide melt. Am. Mineral. 99, 793–803. https://doi.org/10.2138/am.2014.4591.

Howarth, S., Prytulak, J., Little, S.H., Hammond, S.J., Widdowson, M., 2018. Thallium concentration and thallium isotope composition of lateritic terrains. Geochem. Cosmochim. Acta 239, 446–462. https://doi.org/10.1016/j.gca.2018.04.017.

Jakubowska, M., Pasieczna, A., Zembrzuski, W., Świt, Z., Lukaszewski, Z., 2007. Thallium in fractions of soil formed on floodplain terraces. Chemosphere 66, 611–618. https://doi.org/10.1016/j.chemosphere.2006.07.098.

Janković, S.R., Jelenković, R., 1994. Thallium mineralization in the Allchar Sb-As-Tl-Au deposit. N. Jb. Mineral. Abh. 167, 283–297.
Karbowska, B., Zembrzuski, W., Jakubowska, M., Wojtkowiak, T., Pasieczna, A., Lukaszewski, Z., 2014. Translocation and mobility of thallium from zinc-lead ores. J. Geochem. Explor. 143, 127–135. https://doi.org/10.1016/j.gexplo.2014.03.026.
Kersten, M., Xiao, T., Kreissig, K., Brett, A., Coles, B.J., Rehkämper, M., 2014. Tracing anthropogenic thallium in soil using stable isotope compositions. Environ. Sci. Technol. 48, 9030–9036. https://doi.org/10.1021/es501968d.
Kříbek, B., Šípková, A., Ettler, V., Mihaljevič, M., Majer, V., Knésl, I., Mapani, B., Penížek, V., Vaněk, A., Sracek, O., 2018. Variability of the copper isotopic composition in soil and grass affected by mining and smelting in Tsumeb, Namibia. Chem. Geol. 493, 121–135. https://doi.org/10.1016/j.chemgeo.2018.05.035.
Liu, J., Wang, J., Chen, Y., Xie, X., Qi, J., Lippold, H., Luo, D., Wang, C., Su, L., He, L., Wu, Q., 2016. Thallium transformation and partitioning during Pb-Zn smelting and environmental implications. Environ. Pollut. 212, 77–89. https://doi.org/10.1016/j.envpol.2016.01.046.
Liu, J., Yin, M., Luo, X., Xiao, T., Wu, Z., Li, N., Wang, J., Zhang, W., Lippold, H., Belshaw, N.S., Feng, Y., Chen, Y., 2019. The mobility of thallium in sediments and source apportionment by lead isotopes. Chemosphere 219, 864–874.
Liu, J., Yin, M., Xiao, T., Zhang, C., Tsang, D.C.W., Bao, Z., Zhou, Y., Chen, Y., Luo, X., Yuan, W., Wang, J., 2020. Thallium isotopic fractionation in industrial process of pyrite smelting and environmental implications. J. Hazard Mater. 384, 121378 https://doi.org/10.1016/j.jhazmat.2019.121378.
Liu, J., Ouyang, Q., Wang, L., Wang, J., Zhang, Q., Wei, X., Lin, Y., Zhou, Y., Yuan, W., Xiao, T., 2022. Quantification of smelter-derived contributions to thallium contamination in river sediments: novel insights from thallium isotope evidence. J. Hazard Mater. 424, 127594 https://doi.org/10.1016/j.jhazmat.2021.127594.
Liu, J., Wang, L., Lin, J., Yuan, W., Li, L., Peng, Y., Xiong, X., Cao, H., Wei, X., Ouyang, Q., Lippold, H., Wang, J., Lin, K., 2024. Applying thallium isotopic compositions as novel and sensitive proxy for Tl(I)/Tl(III) transformation and source apportionment. Sci. Total Environ. 913, 169542 https://doi.org/10.1016/j.scitotenv.2023.169542.
Lukaszewski, Z., Jakubowska, M., Zembrzuski, W., 2018. The mobility of thallium from bottom soil of the Silesian-Cracowian zinc-lead ore deposit region (Poland). J. Geochem. Explor. 184, 11–16. https://doi.org/10.1016/j.gexplo.2017.10.009.
Mathur, R., Titley, S., Barra, F., Brantley, S., Wilson, M., Phillips, A., Munizaga, F., Maksaev, V., Vervoort, J., Hart, G., 2009. Exploration potential of Cu isotope fractionation in porphyry copper deposits. J. Geochem. Explor. 102, 1–6. https://doi.org/10.1016/j.gexplo.2008.09.004.
Mathur, R., Arribas, A., Megaw, P., Wilson, M., Stroup, S., Meyer-Arrivillaga, D., Arribas, I., 2018. Fractionation of silver isotopes in native silver explained by redox reactions. Geochem. Cosmochim. Acta 224, 313–326. https://doi.org/10.1016/j.gca.2018.01.011.
Milot, J., Blichert-Toft, J., Sanz, M.A., Malod-Dognin, C., Télouk, P., Albarède, F., 2022. Silver isotope and volatile trace element systematics in galena samples from the Iberian Peninsula and the quest for silver sources of Roman coinage. Geology 50, 422–426. https://doi.org/10.1130/G49690.1.
Nielsen, S.G., Wasylenki, L.E., Rehkämper, M., Peacock, C.L., Xue, Z., Moon, E.M., 2013. Towards an understanding of thallium isotope fractionation during adsorption to manganese oxides. Geochem. Cosmochim. Acta 117, 252–265. https://doi.org/10.1016/j.gca.2013.05.004.
Nielsen, S.G., Rehkämper, M., Prytulak, J., 2017. Investigation and application of thallium isotope fractionation. Rev. Mineral. Geochem. 82, 759–798. https://doi.org/10.2138/rmg.2017.82.18.
Pansu, M., Gautheyrou, J., 2006. Handbook of Soil Analysis: Mineralogical, Organic and Inorganic Methods. Springer-Verlag, Berlin, Heidelberg, Germany.
Pavićević, M.K., Bosch, F., Amthauer, G., Aničin, I., Boev, B., Brüchle, W., Djurčić, Z., Faestermann, T., Henning, W.F., Jelenković, R., Pejović, V., 2010. New data for the geochemical determination of the solar pp-neutrino flux by means of lorandite mineral. Nucl. Instrum. Methods A621, 278–285. https://doi.org/10.1016/j.nima.2010.06.090.
Peacock, C.L., Moon, E.M., 2012. Oxidative scavenging of thallium by birnessite: Explanation for thallium enrichment and stable isotope fractionation in marine ferromanganese precipitates. Geochem. Cosmochim. Acta 84, 297–313. https://doi.org/10.1016/j.gca.2012.01.036.
Percival, T., Radtke, A.S., 1994. Sedimentary-rock-hosted dissemination gold mineralization in the Alšar district, Macedonia. Can. Mineral. 32, 649–655.
Phillips, R.F., Wang, Y., Klein, F., Fardan, G., Ostrander, C.M., Gadol, H., Hansel, C.M., Nielsen, S.G., 2023. The role of manganese oxide mineralogy in thallium isotopic fractionation upon sorption. Geochem. Cosmochim. Acta 356, 83–92. https://doi.org/10.1016/j.gca.2023.07.011.
Prytulak, J., Nielsen, S.G., Plank, T., Barker, M., Elliot, T., 2013. Assessing the utility of thallium and thallium isotopes for tracing subduction zone inputs to the Mariana arc. Chem. Geol. 345, 139–149. https://doi.org/10.1016/j.chemgeo.2013.03.003.
Prytulak, J., Brett, A., Webb, M., Plank, T., Rehkämper, M., Savage, P.S., Woodhead, J., 2017. Thallium elemental behavior and stable isotope fractionation during magmatic processes. Chem. Geol. 448, 71–83. https://doi.org/10.1016/j.chemgeo.2016.11.007.
Rehkämper, M., Frank, M., Hein, J.R., Halliday, A., 2004. Cenozoic marine geochemistry of thallium deduced from isotopic studies of ferromanganese crusts and pelagic sediments. Earth Planet Sci. Lett. 219, 77–91. https://doi.org/10.1016/S0012-821X(03)00703-9.
Strmić Palinkaš, S., Hofstra, A.H., Percival, T.J., Borojević Šoštarić, S., Palinkaš, L., Bermanec, V., Pecskay, Z., 2018. Comparison of the allchar Au-as-Sb-Tl deposit, republic of Macedonia, with carlin-type gold deposits. Rev. Econ. Geol. 20, 335–363. https://doi.org/10.5382/rev.20.10.
Vaněk, A., Grösslová, Z., Mihaljevič, M., Trubač, J., Ettler, V., Teper, L., Cabala, J., Rohovec, J., Zádorová, T., Penížek, V., Pavlů, L., Holubík, O., Němeček, K., Houška, J., Drábek, O., Ash, C., 2016. Isotopic tracing of thallium contamination in soils affected by emissions from coal-fired power plants. Environ. Sci. Technol. 50, 9864–9871. https://doi.org/10.1021/acs.est.6b01751.
Tremel, A., Masson, P., Sterckeman, T., Baize, D., Mench, M., 1997. Thallium in French agrosystems-I. thallium contents in arable soils. Environ. Pollut. 95, 293–302. https://doi.org/10.1016/S0269-7491(96)00145-5.
Vaněk, A., Grösslová, Z., Mihaljevič, M., Ettler, V., Trubač, J., Chrastný, V., Penížek, V., Teper, L., Cabala, J., Voegelin, A., Zádorová, T., Oborná, V., Drábek, O., Holubík, O., Houška, J., Pavlů, L., Ash, C., 2018. Thallium isotopes in metallurgical wastes/contaminated soils: a novel tool to trace metal source and behavior. J. Hazard Mater. 343, 78–85. https://doi.org/10.1016/j.jhazmat.2017.09.020.
Vaněk, A., Voegelin, A., Mihaljevič, M., Ettler, V., Trubač, J., Drahota, P., Vaňková, M., Oborná, V., Vejvodová, K., Penížek, V., Pavlů, L., Drábek, O., Vokurková, P., Zádorová, T., Holubík, O., 2020. Thallium stable isotope ratios in naturally Tl-rich soils. Geoderma 364, 114183. https://doi.org/10.1016/j.geoderma.2020.114183.
Vejvodová, K., Vaněk, A., Mihaljevič, M., Ettler, V., Trubač, J., Vaňková, M., Drahota, P., Vokurková, P., Penížek, V., Zádorová, T., Tejnecký, V., Pavlů, L., Drábek, O., 2020. Thallium isotopic fractionation in soil: the key controls. Environ. Pollut. 265, 114822 https://doi.org/10.1016/j.envpol.2020.114822.
Vejvodová, K., Vaněk, A., Drábek, O., Spasić, M., 2022. Understanding stable Tl isotopes in industrial processes and the environment: a review. J. Environ. Manag. 315, 115151 https://doi.org/10.1016/j.jenvman.2022.115151.
Voegelin, A., Pfenninger, N., Petrikis, J., Majzlan, J., Plötze, M., Senn, A.C., Mangold, S., Steininger, R., Göttlicher, J., 2015. Thallium speciation and extractability in a thallium- and arsenic-rich soil developed from mineralized carbonate rock. Environ. Sci. Technol. 49, 5390–5398. https://doi.org/10.1021/acs.est.5b00629.
Volkov, A.V., Serafimovski, T., Kochneva, N.T., Tomson, I.N., Tasev, G., 2006. The Alshar epithermal Au-As-Sb-Tl deposit, southern Macedonia. Geol. Ore Deposits 48, 175–192. https://doi.org/10.1134/S1075701506030020.
Wang, D., Mathur, R., Zheng, Y., Wu, H., Lv, Y., Zhang, G., Huan, R., Yu, M., Li, Y., 2022. Constraints on ore-forming fluid evolution and guidance for ore exploration in the Zhaxikang Sb-Pb-Zn-Ag deposit in southern Tibet: insights from silver isotope fractionation of galena. Miner. Deposita 57, 701–724. https://doi.org/10.1007/s00126-022-01111-5.
Wei, X., Wang, J., She, J., Sun, J., Liu, J., Wang, Y., Yang, X., Ouyang, Q., Lin, Y., Xiao, T., Tsang, D.C.W., 2021. Thallium geochemical fractionation and migration in Tl-As rich soils: the key controls. Sci. Total Environ. 784, 146995 https://doi.org/10.1016/j.scitotenv.2021.146995.
Wick, S., Peña, J., Voegelin, A., 2019. Thallium sorption onto manganese oxides. Environ. Sci. Technol. 53, 13168–13178. https://doi.org/10.1021/acs.est.9b04454.
Wick, S., Baeyens, B., Fernandes, M.M., Göttlicher, J., Fischer, M., Pfenninger, N., Plötze, M., Voegelin, A., 2020. Thallium sorption and speciation in soils: role of micaceous clay minerals and manganese oxides. Geochem. Cosmochim. Acta 288, 83–100. https://doi.org/10.1016/j.gca.2020.07.037.
Xiao, T., Guha, J., Boyle, D., Liu, C.Q., Zheng, B., Wilson, G.C., Rouleau, A., Chen, J., 2004a. Naturally occurring thallium: a hidden geoenvironmental health hazard? Environ. Int. 30, 501–507. https://doi.org/10.1016/j.envint.2003.10.004.
Xiao, T., Guha, J., Boyle, D., 2004b. High thallium content in rocks associated with Au–As–Hg-Tl and coal mineralization and its adverse environmental potential in SW Guizhou, China. Geochem. Explor. Environ. Anal. 4, 243–252. https://doi.org/10.1144/1467-7873/04-204.
Xiao, T., Yang, F., Li, S., Zheng, B., Ning, Z., 2012. Thallium pollution in China: a geo-environmental perspective. Sci. Total Environ. 421–422, 51–58.